Vertically Aligned BCN Nanotubes with High Capacitance

Eswaramoorthi Iyyamperumal,[†] Shuangyin Wang,[†] and Liming Dai*

Center of Advanced Science and Engineering for Carbon (Case4Carbon), Department of Macromolecular Science and Engineering, Case Western Reserve University, 10900 Euclid Avenue, Cleveland, Ohio 44106, United States. [†]These authors contributed equally.

ABSTRACT

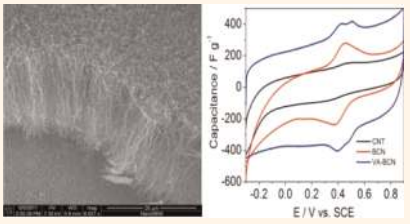

Using a chemical vapor deposition method, we have synthesized vertically aligned BCN nanotubes (VA-BCNs) on a Ni–Fe-coated SiO_2/Si substrate from a melamine diborate precursor. The effects of pyrolysis conditions on the morphology and thermal property of grown nanotubes, as well as the nanostructure and composition of an individual BCN nanotube, were systematically studied. It was found that nitrogen atoms are bonded to carbons in both graphitic and pyridinic forms and that the resultant VA-BCNs grown at 1000 °C show the highest specific capacitance (321.0 F/g) with an excellent rate capability and high durability with respect to nonaligned BCN (167.3 F/g) and undoped multiwalled carbon nanotubes (117.3 F/g) due to synergetic effects arising from the combined co-doping of B and N in CNTs and the well-aligned nanotube structure.

KEYWORDS: BCN nanotubes · supercapacitance · co-doping · CVD synthesis · aligned nanotubes

Along with carbon nanotubes (CNTs), hexagonal boron nitride (BN) and boron carbonitride (BCN) nanotubes have been extensively studied due to their nearly the same lattice parameters as those of graphite and their unique electronic and thermal properties attractive for various potential applications, including electronics, electrical conductors, high-temperature lubricants, and novel composites.[1–4] Of particular interest, BCN nanotubes, in which carbon atoms are partially substituted by boron and nitrogen atoms, possess unique electrical and thermal properties determined mainly by their atomic composition and configuration. The band gaps of BCN nanotubes are known to be intermediate between semimetallic graphite and insulating hexagonal BN.[5] Therefore, the electronic properties of BCN nanotubes can be relatively more easily controlled by adjusting their composition and the arrangement of B, C, and N atoms rather than by chirality control in CNTs.[6,7]

Different methods, such as laser ablation,[8] pyrolysis,[9] bias-assisted hot-filament chemical vapor deposition (CVD),[10,11] aerosol-assisted CVD and laser vaporization process,[12] and dc arc discharge[13] using different B, C, and N sources, have been reported for the synthesis of BCNs or nanotubes with separated phases of BN and C. Shelimov and Moskovits[14] first reported the formation of arrays of C/BN/C nanotubules with larger diameter (270–360 nm) by pyrolyzing acetylene and trichloroborazine over a porous anodic alumina template. Meanwhile, bias-assisted hot filament CVD was used to grow aligned BCN nanotubes from B_2H_6, CH_4, N_2, and H_2[5] and aligned Y-shaped BCN nanojunctions through a pause–reactivation two-stage process.[15] In the latter case, the composition of the nanotube junction was tailored simply by varying the concentration of gaseous precursors (CH_4, B_2H_6, and N_2) between the two stages of the growth process.[15] Pyrolysis of melamine with boron oxide at 1150 °C in the presence of ferrocene resulted in uniform array of aligned BCN nanotubes with varying composition.[16] In addition, aligned multiwalled BCN/CNT junctions with a typical rectifying diode behavior were also produced by the hot-filament CVD method from the CH_4, N_2, and B_2H_6 precursor and Ni catalyst.[17] Recently, we have produced vertically aligned (VA)-BCN nanotubes by pyrolysis of melamine diborate, a single compound containing carbon, boron, and nitrogen sources required for the BCN nanotube growth.[18] The use of a single-compound precursor is of particular interest, as it simplifies the nanotube growth process. While the growth conditions for the VA-BCN nanotubes have been reported briefly in our previous publication,[18] the

* Address correspondence to liming.dai@case.edu.

Received for review March 8, 2012 and accepted May 28, 2012.

Published online May 28, 2012
10.1021/nn301044v

effects of pyrolysis conditions (*e.g.*, temperature) on the morphology and thermal property of grown nanotubes as well as the nanostructure and composition of an individual BCN nanotube are systematically studied in the present work, along with the first demonstration of their application in supercapacitors.

Having a high power density, quick charge/discharge rate, and long life-cycle,[19−21] supercapacitors are promising power sources for portable systems and automotive applications. Supercapacitance arises normally from the electrical double-layer charge storage with or without additional pseudocapacitance.[22] Carbon nanomaterials such as CNTs, graphene, and ordered mesoporous carbon are considered as typical electrode materials for electric double-layer capacitors (EDLC), and much attention has been paid to improve their structure and properties for capacitor applications.[22] In spite of their moderate surface area compared to activated carbons, CNTs show reasonably high capacitances due to their large mesoporosity for high electrolyte accessibility and excellent electrical conductivity and, hence, a high power density for the electrochemical capacitor.[22] However, the electrochemical behavior of randomly entangled CNT electrodes showed a rather limited capacitance compared to the vertically aligned carbon nanotube (VA-CNT) arrays.[23−28] Unlike VA-CNT arrays, the randomly entangled CNTs are most likely unable to support a facilitated access of the electrolyte ions due to the mismatch between the irregular pore structures. Alternatively, the supercapacitor performance can also be enhanced by chemical functionalization of carbon materials with various heteroatoms, which could provide redox characteristics for improved pseudocapacitance. Indeed, oxygen-doping of porous carbons has been demonstrated to significantly enhance the specific capacitance up to 220 F/g,[29] as does nitrogen-doping (300 F/g).[30] A similar, but independent, study showed that N and B co-doping of porous carbon could enhance its specific capacitance up to 268 F/g due to a synergistic pseudocapacitive effect.[31] Herein, we report an unusually high supercapacitance (321 F/g) for our newly developed VA-BCN nanotubes even without postsynthesis functionalization. Compared with the nonaligned BCN nanotubes and undoped CNTs, VA-BCN nanotubes show the highest specific capacitance with an excellent rate capability and high durability, and thus are attractive as electrode materials for supercapacitor applications. The observed high supercapacitance can be attributed to the combined effects of the nanotube alignment and B-/N-co-doping mentioned above.

RESULTS AND DISCUSSION

Figure 1 shows typical SEM images of VA-BCN nanotubes grown at different temperatures. It is clearly seen that vertically aligned nanotubes with high packing densities are grown on the SiO_2/Si substrate. Also, the alignment degree and length of the nanotubes vary with the pyrolysis temperature. The length of the nanotubes is found to increase with increasing pyrolysis temperature. The lengths of the nanotubes grown at 900, 950, and 1000 °C are around 10, 15, and 20 μm, respectively. The nanotubes grown at 900 °C show a relatively poor alignment, whereas a very good alignment is observed for the nanotubes grown at 1000 °C. The corresponding SEM image for the nonaligned BCN nanotubes is shown in Figure S1 in the Supporting Information.

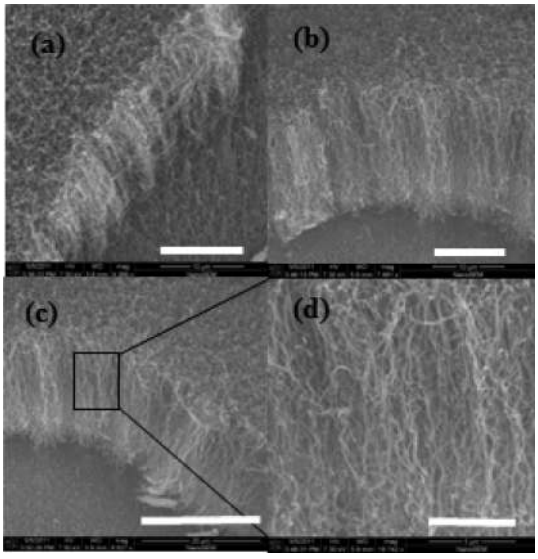

Figure 1. SEM images of VA-BCN nanotubes grown at different temperatures over Ni−Fe-coated SiO_2/Si substrates, (a) 900 °C, (b) 950 °C, and (c) 1000 °C, and (d) high-magnification view of (c) showing the vertical alignment of nanotubes. Scale bars: (a) 10 μm, (b) 10 μm, (c) 20 μm, (d) 5 μm.

As can be seen in Figure 2a, the thermal stability in air for the VA-BCN nanotubes grown at different temperatures increased with increasing synthesis temperature. BCN nanotubes grown at 1000 °C are found to be almost stable up to 900 °C in air. The observed thermal decomposition around 550 °C for VA-BCN nanotubes grown at 900 and 950 °C is attributable to the oxidation of amorphous carbon layers co-deposited on the BCN nanotubes at relatively low deposition temperatures.[32] The slight weight gain seen above 800 °C is, most probably, due to the oxidation of catalyst Fe−Ni particles present in the nanotubes.

The Raman spectra of VA-BCN nanotubes grown at different temperatures given in Figure 2b reveal that all the nanotubes showed characteristic D-, G-, and 2D-bands, indicating the graphitic structure. The first-order peaks include a D-band located around 1342 cm^{-1} and a G-band around 1570 cm^{-1}. The higher order peak appeared at 2670 cm^{-1}, and a small broad peak at 2910 cm^{-1} can be assigned to a combination of D+D and D+G bands.[33] The G-band arises

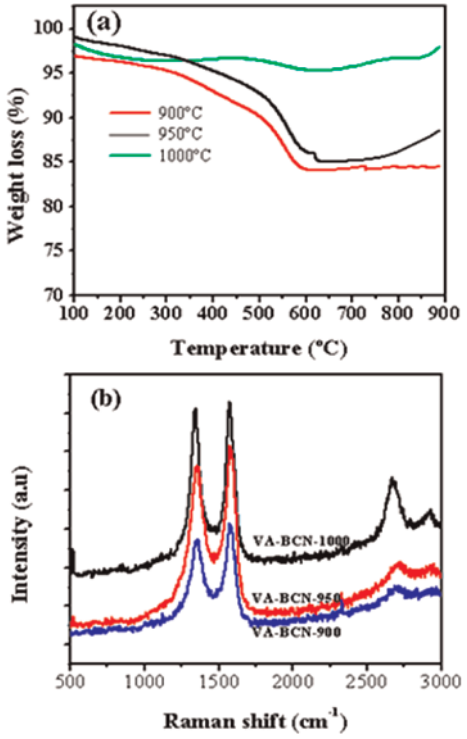

Figure 2. (a) TGA profiles measured in air and (b) Raman spectra of VA-BCN nanotubes grown at different temperatures (excitation wavelength: 514 nm).

from stretching of all sp^2-bonded pairs, including C−C, B−C, N−C, and B−N, while the D-band is associated with the sp^3 defect sites.[34] The I_D/I_G value is found to increase from 0.86 to 0.97 when increasing the pyrolysis temperature from 900 to 1000 °C. The observed I_D/I_G values agree well with the reported values for BCN nanotubes, which range from 0.68 for $B_{0.11}C_{0.85}N_{0.04}$ to 1.10 for $B_{0.26}C_{0.57}N_{0.17}$.[35] When increasing the pyrolysis temperature, therefore, more defects are created due to more B and N atoms doped into the graphitic network. Also, the intensities of 2D (2670 cm^{-1}) and D+G (2910 cm^{-1}) bands increased with increasing pyrolysis temperature, confirming that more B and N atoms are doped in the CNTs.[33] On the basis of the SEM, TGA, and Raman studies, the VA-BCN nanotubes grown at 1000 °C seem to be more suitable than their counterparts synthesized at lower temperatures for energy-related applications.[22] In order to study the nanotube quality, the XRD patterns of VA-BCN nanotubes grown at different temperatures were recorded (Figure S2 in Supporting Information). Two characteristic peaks at 2θ values of 26.3° and 43.6°, respectively, for (002) and (100) plane reflections were observed, indicating the well-graphitized nature of the grown nanotubes. The peak intensity at 26.3° increased with increasing growth temperature, suggesting a better quality for the VA-BCN array grown at 1000 °C than those grown at lower temperatures, consistent with TGA and Raman measurements. The other small peaks seen in Figure S2 are from the SiO_2/Si substrate used to

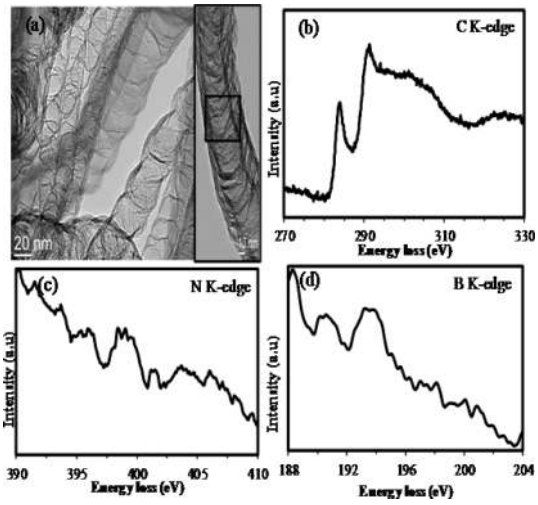

Figure 3. (a) Typical TEM image and EELS spectrum of (b) C, (c) N, and (d) B K-edges of VA-BCN nanotubes grown at 1000 °C on a Ni−Fe-coated SiO_2/Si substrate.

grow the nanotubes. Furthermore, the specific surface area of the VA-BCN array grown at 1000 °C was measured. The N_2 physisorption showed a typical type II isotherm (Figure S3 in Supporting Information), characteristic of multiwalled CNTs, with a relatively high BET surface area (347 m^2/g).

The morphology of the aligned BCN nanotube grown at 1000 °C was imaged by TEM. A typical image is given in Figure 3 along with EELS spectra for K-edges of C, B, and N. It is clearly seen that the resultant nanotubes are 25−35 nm in diameter (Figure 3a). The typical bamboo-like structure is clearly seen, and the wall thickness is around 10 nm, indicating a multiwalled nature for the BCN nanotubes similar to those reported in the previous publications.[11,36] Tubular structures with transverse connections across the inner walls of the nanotubes are also clearly seen in the inset of Figure 3a.

The presence of C, B, and N in the grown nanotubes was confirmed by EELS analysis of the K-edges of C, B, and N on a single nanotube, shown in Figure 3. The obtained typical C, B, and N K-edge spectra are given in Figure 3b−d, respectively. In the case of the C K-edge (Figure 3b), two characteristic high-intensity peaks at 284.7 and 292.2 eV confirm the presence of graphitic carbon in the nanotube. These two peaks are attributed to a 1s−π^* transition and a series of 1s−σ^* transitions, respectively. The shape and position of the peaks indicate the well-graphitized nature of BCN nanotubes. The presence of trivalent nitrogen in the graphitic hexagonal lattice[37] was shown by a broad peak around 400 eV, as shown in Figure 3c. The peak for nitrogen is relatively weak and broad with respect to the high-intensity C K-edge observed around 280−330 eV. Figure 3d exhibits two pronounced peaks for the B K-edge at about 191 and 194 eV, confirming the sp^2 hybridization state of B atoms. The low-energy

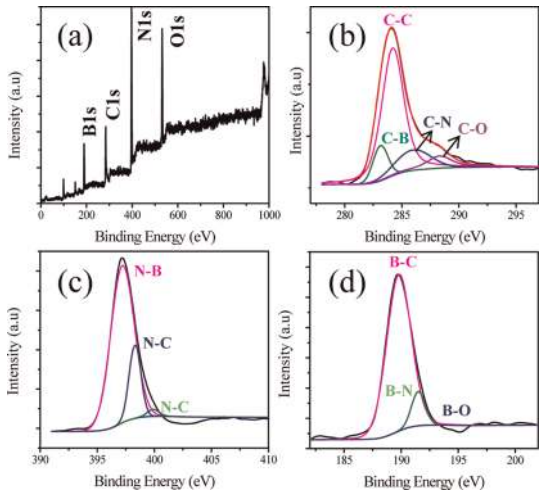

Figure 4. XPS spectra of VA-BCN nanotubes grown at 1000 °C: (a) survey spectrum and high-resolution spectrum of (b) C 1s, (c) N 1s, and (d) B 1s.

peak (191 eV) can be accounted for boron bonded to carbon, and the high-energy peak (194 eV) originates from boron bonded to nitrogen.[38] The low peak intensity for the B K-edge may be due to the smaller boron content in the nanotubes. These results clearly revealed that the resultant nanotubes are made up of B, C, and N.

The chemical composition of the vertically aligned BCN nanotubes grown at 1000 °C was further analyzed by X-ray photoelectron spectroscopy (XPS). The percentage of B, C, and N in the as-grown BCN nanotubes was calculated from the XPS survey spectrum (Figure 4a) to be around 27%, 25%, and 31%, respectively. The Si signal around 100 eV originated from the SiO_2/Si substrate, and the oxygen signal around 540 eV is from both substrate and physically adsorbed O_2 on the nanotubes.[39] The predominant asymmetric C 1s peak shown in Figure 4b indicates the existence of C−N or C−B bonds in the graphitic network. The four deconvoluted peaks in the C 1s spectrum at 283.4, 284.7, 286.2, and 288.3 eV could be assigned to C−B, C−C, C−N, and C−O bonds, respectively. As can be seen in Figure 4b, the percentage of C bonded to B is significantly higher than that of C bonded to N or O species. The high-resolution N 1s XPS peak in Figure 4c could be deconvoluted into three subpeaks at 397.2, 398.4, and 399.9 eV, attributable to the N−B bond, graphitic N−C bond, and pyridinic N−C bond, respectively. The amount of pyridinic N is relatively smaller than the graphitic nitrogen. The high-resolution and deconvoluted B 1s XPS spectrum given in Figure 4d shows mainly two subpeaks at 189.8 and 191.5 eV, arising from the B−C and B−N bond, respectively. The relatively higher intensity of the B−C peak than that of B−N indicates that a greater number of B is attached to C in the network.

Cyclic voltammetry and galvanostatic charge/discharge curves (Figure 5 and Figure 6) from both

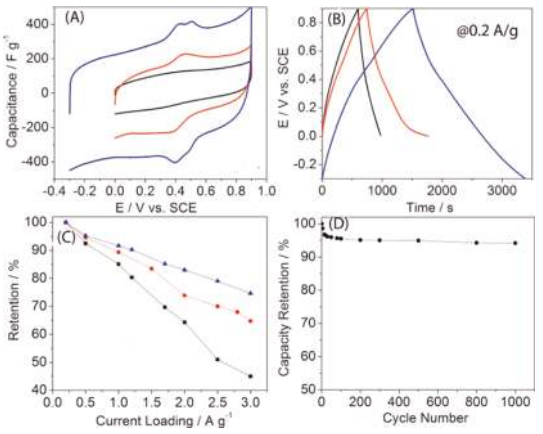

Figure 5. (A) CV curves of CNT (black), BCN (red), and VA-BCN (blue) samples in 1 M H_2SO_4 solution at a scan rate of 5 mV/s; (B) charge/discharge curves of CNT (black), BCN (red), and VA-BCN (blue) samples in 1 M H_2SO_4 solution at a current density of 0.2 A/g; (C) corresponding capacity retentions at the current density from 0.2 to 3 A/g; (D) stability evaluation of the VA-BCN electrode material in 1 M H_2SO_4 solution at a charge current of 1 A/g.

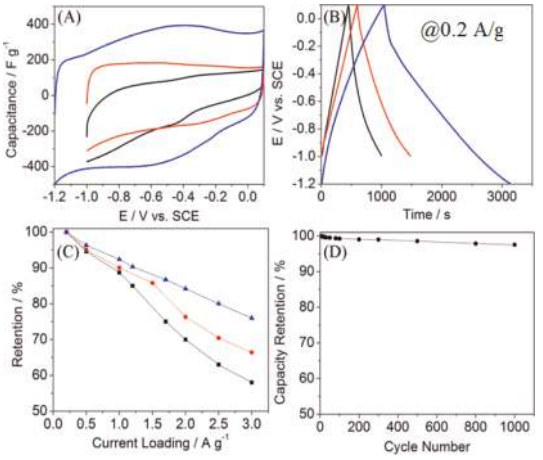

Figure 6. (A) CV curves of CNT (black), BCN (red), and VA-BCN (blue) samples in 6 M KOH solution at a scan rate of 5 mV/s; (B) charge/discharge curves of CNT (black), BCN (red), and VA-BCN (blue) samples in 6 M KOH solution at a current density of 0.2 A/g; (C) corresponding capacity retentions at the current density from 0.2 to 3 A/g; (D) stability evaluation of the VA-BCN electrode material in 6 M KOH solution at a charge current of 1 A/g.

acidic (1 M H_2SO_4) and basic (6 M KOH) media were used to characterize the capacitive properties in this study. The voltammetry characteristics and galvanostatic charge/discharge cycles show good capacitive response even at a high current loading (1A/g). Figure 5A shows typical cyclic voltammograms (CV) for a three-electrode cell in 1 M H_2SO_4 at a scan rate of 5 mV/s. The CNT sample exhibits a small rectangular curve corresponding to a low capacitance. The non-aligned BCN nanotubes present a typical capacitive behavior with a rectangular-like shape of the voltammetry characteristics. The rectangular-like shape and the appearance of humps in the CV curves indicate that the capacitive response comes from the combination

of EDLC and redox reactions related to the heteroatom functionalities. It has been previously proposed that heteroatom doping could change the electronic properties of carbon materials with the doped heteroatoms in the carbon materials being more favorable to attract ions in the electrolyte compared to that of carbon atoms, which would introduce the pseudocapacitance.[30,31] That is why clear humps are observed in the CV curves on BCN samples. In addition, the heteroatom doping can also improve the electric double-layer capacitance, as evidenced by the bigger CV loop observed for the BCN electrode than that of the CNT electrode (*e.g.*, Figure 5A), indicating a thicker double-layer region for the BCN electrode. This is because the presence of heteroatoms in the carbon matrix can enhance the wettability (hydrophilicity) between electrolyte and electrode materials. Therefore, the heteroatom doping could not only introduce extra pseudocapacitance but also enhance the electric double-layer capacitance. It is interesting to observe that the electrochemical potential window of VA-BCN is wider compared with the other two samples. The CV curves were also scanned at the same potential window for nonaligned BCN and CNT samples, but they showed very poor rectangular quality (Figures S4 and S5). The observed wide electrochemical potential window could lead to a high power density and energy density[22] for supercapacitors based on the VA-BCN electrode materials. The redox reactions can also be observed in the galvanostatic charge/discharge curves (Figure 5B and Figure 6B). Unlike linear characteristics, a transition can be easily noticed between 0.3 and 0.5 V in the acidic electrolyte. The small transition in line slopes around 0.4 V correlates with the redox peaks in the CV curves. The specific capacitances (*C*) were calculated from galvanostatic charge/discharge curves according to *It*/*E*, where *I* is the charge/discharge current, *t* the discharge time, and *E* the voltage difference. From the galvanostatic charge/discharge curves in Figure 5B, the specific capacitance of the VA-BCN electrode in 1 M H_2SO_4 was found to be around 312.0 F/g, which is significantly higher than that of nonaligned BCN (162.5 F/g) and multiwall CNT (83.8 F/g). The relatively high capacitance of BCN compared to CNT is due to the pseudocapacitive effect associated with the heteroatom functionality. On the other hand, because of its well-defined aligned structure, VA-BCN showed the highest specific capacitance. This is because the aligned morphology of VA-BCN could effectively facilitate the transportation of electrolyte ions during the charge/discharge process and, thus, improve the supercapacitance. Therefore, both the presence of heteroatoms (B and N) and the aligned structures contribute to the observed high specific capacitance for VA-BCN nanotubes.

Figure 5C represents the relationships between specific capacitance and charge/discharge current density to study the rate capability of the electrode materials. The capacitance retention is defined as the ratio of the specific capacitance at various current densities to that at 0.2 A/g. When the charge/discharge current density was increased from 0.2 to 3 A/g, the capacitance retention of a CNT was only 45%, which is significantly lower than that of the BCN (65%) and VA-BCN (76%). Clearly, therefore, the incorporation of B and N into the CNTs and the aligned structure have remarkably improved the capacitance performance of electrodes at high charge/discharge rate, and this is very important for the applications where a high rate of discharge−recharge is required. Long cycling life is another important requirement for supercapacitors. In this context, the cycling life test for the VA-BCN electrode was carried out by repeating the charge/discharge test at a current density of 1 A/g for 1000 cycles. Figure 5D shows the capacitance retention ratio of the capacitor electrode charged at 1 A/g as a function of the cycle number. As can be seen, the electrode exhibited an excellent electrochemical stability with only 5% deterioration of the initial available specific capacitance after 1000 cycles.

In addition, we have also investigated the electrochemical behavior of the three electrode materials in basic media (6 M KOH), and the results are shown in Figure 6, which also shows a wider electrochemical potential window, the highest specific capacitance, better rate capability, and excellent electrochemical stability for the VA-BCN electrode. The specific capacitance of the VA-BCN electrode in 6 M KOH is around 321.0 F/g, a value that is significantly higher than that of BCN (167.3 F/g) and multiwalled CNT (117.3 F/g). Comparing to the acidic electrolyte solution, the supercapacitor performance in the basic medium is better, as the working potential in acidic medium is relatively higher. However, the difference in specific capacitance between the basic and acidic media for the VA-BCN electrode (9 F/g) and BCN (5F/g) is much smaller than that of the undoped CNT (33 F/g), indicating that VA-BCN and BCN nanotubes work well in both acidic and basic media due to the synergetic co-doping of B and N and well-aligned nanotube structure in the electrode materials.

CONCLUSIONS

Vertically aligned BCN nanotubes were grown by pyrolysis of melamine diborate at different temperatures on Ni−Fe-coated SiO_2/Si substrates. The structure and capacitive properties of the vertically aligned BCN nanotubes, along with the nonaligned BCN, and pure carbon nanotubes (CNT) were systematically studied. Vertically aligned BCN nanotubes grown at 1000 °C are found to be thermally more stable than those grown at lower temperatures, while the Raman spectroscopy revealed that pyrolysis at a higher temperature increased the number of B and N atoms doped into the graphitic network. Both the B and N

co-doping effect and the structure alignment were found to enhance the supercapacitor property of vertically aligned BCN nanotubes in comparison with nonaligned BCN and undoped multiwalled CNTs. The vertically aligned BCN nanotubes grown at 1000 °C showed the highest specific capacitance (321.0 F/g) with respect to nonaligned BCN (167.3 F/g) and undoped multiwalled carbon nanotubes (117.3 F/g), with an excellent rate capability and high durability due to synergetic effects arising from the combined co-doping of B and N in CNTs and well-aligned nanotube structure.

EXPERIMENTAL SECTION

Melamine diborate, synthesized by reacting melamine with boric acid, was used as a precursor for the CVD synthesis of vertically aligned multiwall BCN nanotubes. For the synthesis of melamine diborate, melamine (1 mmol) was dissolved in deionized water at 80 °C, to which boric acid (2 mmol) was added slowly under stirring for 30 min. The mixture solution was then cooled slowly to allow complete precipitation of melamine diborate, followed by filtration and drying at 80 °C overnight. Thereafter, VA-BCN nanotubes were grown on a sputter-coated Fe/Ni layer (5 nm/5 nm thick) on a commercial SiO_2/Si substrate (Siliconquest). The precursor melamine diborate in a ceramic boat and Ni–Fe-coated SiO_2/Si substrate were placed separately inside a quartz reactor. The temperature of the furnace was ramped to 1000 °C under Ar/H_2 flow (50 cc/min), while the melamine diborate and substrate were placed at the lower temperature region of the reactor. After introducing nitrogen gas (50 cm^3/min) into the tube furnace, the melamine diborate and SiO_2/Si substrate were quickly moved to the region of 1000 °C for 10 min to grow VA-BCN nanotubes on the SiO_2/Si substrate. Finally, the substrate-supported VA-BCN nanotube array was removed quickly away from the reaction zone and cooled under Ar flow. In order to optimize the growth conditions for well-aligned long BCN nanotubes, similar experiments were carried out at 900 and 950 °C. For comparison purposes, nonaligned BCN nanotubes were grown under similar conditions at 1000 °C using 1 wt % Ni and Co containing melamine diborate. Similarly, the vertically aligned undoped CNTs were grown at 850 °C on a Ni–Fe sputter-coated SiO_2/Si substrate using ethylene as carbon source. The morphology of the aligned BCN nanotubes grown at different temperatures was analyzed by scanning electron microscopy (SEM). The vibrational characteristics of BCN nanotubes grown at different temperatures were analyzed by Raman spectroscopy (Renishaw), using a 514 nm excitation wavelength laser. Thermogravimetric analysis (TGA) was carried out on a TA Instruments apparatus with a heating rate of 10 °C in air. High-resolution TEM images were acquired with a Zeiss LIBRA 200FE transmission electron microscope equipped with EELS using BCN nanotubes dispersed over holey carbon-coated Cu grids. The C, N, and B K-edge spectra from a spot on a single BCN nanotube were acquired to determine the composition of the nanotubes. X-ray photoelectron spectroscopic measurements were performed on a VG Microtech ESCA 2000 using a monochromic Al X-ray source (97.9 W, 93.9 eV). X-ray diffraction (XRD) was measured on a Rigaku X-ray diffractometer. The Brunauer–Emmet–Teller (BET) specific surface area was determined from N_2 adsorption at the liquid nitrogen temperature (Micromeritics 2000 ASAP). For electrochemical characterization, a three-electrode glass cell with Pt wire and saturated calomel electrode as counter electrode and reference electrode, respectively, were used. The capacitance was measured in a 6 M KOH and 1 M H_2SO_4 solution, separately.

Conflict of Interest: The authors declare no competing financial interest.

Supporting Information Available: SEM of nonaligned BCN nanotubes, XRD pattern, and N_2 adsorbed isotherm of aligned BCN nanotubes, and CV data of BCN nanotube in H_2SO_4 and KOH along with pure CNTs and nonaligned BCN nanotubes. This material is available free of charge *via* the Internet at http://pubs.acs.org.

Acknowledgment. The authors gratefully acknowledge the financial support from AFOSR, DOD-MURI, AFOSR-AOARD, AFRL/UTC, DAGSI, NSF, and NSF-NSFC.

REFERENCES AND NOTES

1. Stephan, O.; Ajayan, P. M.; Colliex, C.; Redlich, Ph.; Lambert, J. M.; Bernier, P.; Lefin, P. Doping Graphitic and Carbon Nanotube Structures with Boron and Nitrogen. *Science* **1994**, *266*, 1683–1685.
2. Wengsieh, Z.; Cherrey, K.; Chopra, N. G.; Blase, X.; Miyamoto, Y.; Rubio, A.; Cohen, M. L.; Louie, S. G.; Zettl, A.; Gronsky, A. R. Synthesis of $B_xC_yN_z$ Nanotubules. *Phys. Rev. B* **1995**, *51*, 11229–11232.
3. Dai, L. Advanced Syntheses and Microfabrications of Conjugated Polymers, C60 Containing Polymers and Carbon Nanotubes for Optoelectronic Applications. *Polym. Adv. Technol.* **1999**, *10*, 357–420.
4. Wang, W. L.; Bai, X. D.; Liu, K. H.; Xu, Z.; Golberg, D.; Bando, Y.; Wang, E. G. Direct Synthesis of B-C-N Single-Walled Nanotubes by Bias-Assisted Hot Filament Chemical Vapor Deposition. *J. Am. Chem. Soc.* **2006**, *128*, 6530–6531.
5. Bai, X.; Wang, E.; Yu, J.; Yang, H. Blue–Violet Photoluminescence from Large-Scale Highly Aligned Boron Carbonitride Nanofibers. *Appl. Phys. Lett.* **2000**, *77*, 67–69.
6. Miyamoto, Y.; Rubio, A.; Cohen, M. L.; Louie, S. G. Chiral Tubules of Hexagonal BC_2N. *Phys. Rev. B* **1994**, *50*, 4976–4979.
7. Blase, X.; Charlier, J.-C.; De Vita, A.; Car, R. Theory of Composite $B_xC_yN_z$ Nanotubes Heterojunctions. *Appl. Phys. Lett.* **1997**, *70*, 197–199.
8. Zhang, Y.; Gu, H.; Suenaga, K.; Iijima, S. Heterogeneous Growth of B-C-N Nanotubes by Laser Ablation. *Chem. Phys. Lett.* **1997**, *279*, 264–269.
9. Terrones, M.; Benito, A. M.; Manteca-Diego, C.; Hsu, W. K.; Osman, O. I.; Hare, J. P.; Reid, D. G.; Terrones, H.; Cheetham, A. K.; Prassides, K.; *et al*. Pyrolytically Grown $B_xC_yN_z$ Nanomaterials: Nanofibres and Nanotubes. *Chem. Phys. Lett.* **1996**, *257*, 576–582.
10. Yu, J.; Ahn, J.; Yoon, S. F.; Zhang, Q.; Rusli; Gan, B.; Chew, K.; Yu, M. B.; Bai, X. D.; Wang, E. G. Semiconducting Boron Carbonitride Nanostructures: Nanotubes and Nanofibers. *Appl. Phys. Lett.* **2000**, *77*, 1949–1951.
11. Zhi, C. Y.; Guo, J. D.; Bai, X. D.; Wang, E. G. Adjustable Boron Carbonitride Nanotubes. *J. Appl. Phys.* **2002**, *91*, 5325–5333.
12. Enouz-Vedrenne, S.; Stephan, O.; Glerup, M.; Cochon, J.-L.; Colliex, C.; Loiseau, A. Effect of the Synthesis Method on the Distribution of C, B, and N Elements in Multiwall Nanotubes: A Spatially Resolved Electron Energy Loss Spectroscopy Study. *J. Phys. Chem. C* **2008**, *112*, 16422–16430.
13. Piazza, F.; Nocua, J. E.; Hidalgo, A.; De Jesus, J.; Velazquez, R.; Weiss, B. L.; Morell, G. Formation of Boron Carbonitride Nanotubes from *In-Situ* Grown Carbon Nanotubes. *Diamond Relat. Mater.* **2005**, *14*, 965–969.
14. Shelimov, K. B.; Moskovits, M. Composite Nanostructures Based on Template-Grown Boron Nitride Nanotubules. *Chem. Mater.* **2000**, *12*, 250–254.
15. Guo, J. D.; Zhi, C. Y.; Bai, X. D.; Wang, E. G. Boron Carbonitride Nanojunctions. *Appl. Phys. Lett.* **2002**, *80*, 124–126.

16. Han, W.-Q.; Cumings, J.; Zettl, A. Pyrolytically Grown Arrays of Highly Aligned $B_xC_yN_z$ Nanotubes. *Appl. Phys. Lett.* **2001**, *78*, 2769–2771.
17. Liao, L.; Liu, K.; Wang, W.; Bai, X.; Wang, E.; Liu, Y.; Li, J.; Liu, C. Multiwall Boron Carbonitride/Carbon Nanotube Junction and Its Rectification Behavior. *J. Am. Chem. Soc.* **2007**, *129*, 9562–9563.
18. Wang, S.; Iyyamperumal, E.; Roy, A.; Xue, Y.; Yu, D.; Dai, L. Vertically Aligned BCN Nanotubes as Efficient Metal-Free Electrocatalysts for the Oxygen Reduction Reaction: A Synergetic Effect by Co-Doping with Boron and Nitrogen. *Angew. Chem., Int. Ed.* **2011**, *50*, 11756–11760.
19. Lota, G.; Centeno, T. A.; Frackowiak, E.; Stoeckli, F. Improvement of the Structural and Chemical Properties of a Commercial Activated Carbon for Its Application in Electrochemical Capacitors. *Electrochim. Acta* **2008**, *53*, 2210–2216.
20. Frackowiak, E. Carbon Materials for Supercapacitor Application. *Phys. Chem. Chem. Phys.* **2007**, *9*, 1774–1785.
21. Pandolfo, A. G.; Hollenkamp, A. F. Carbon Properties and Their Role in Supercapacitors. *J. Power Sources* **2006**, *157*, 11–27.
22. Dai, L.; Chang, D. W.; Baek, J.-B.; Lu, W. Carbon Nanomaterials for Advanced Energy Conversion and Storage. *Small* **2012**, *8*, 1130–1166.
23. Lee, K. T.; Tsai, C. B.; Ho, W. H.; Wu, N. L. Superabsorbent Polymer Binder for Achieving MnO_2 Supercapacitors of Greatly Enhanced Capacitance Density. *Electrochem. Commun.* **2010**, *12*, 886–889.
24. Wang, S.; Jiang, S. P.; Wang, X. Microwave-Assisted One-Pot Synthesis of Metal/Metal Oxide Nanoparticles on Graphene and Their Electrochemical Applications. *Electrochim. Acta* **2011**, *56*, 3338–3344.
25. Wang, H.; Hao, Q. L.; Yang, X.; Lu, L. D.; Wang, X. Graphene Oxide Doped Polyaniline for Supercapacitors. *Electrochem. Commun.* **2010**, *11*, 1158–1161.
26. Zhang, K.; Zhang, L. L.; Zhao, X. S.; Wu, J. S. Graphene/Polyaniline Nanoriber Composites as Supercapacitor Electrodes. *Chem. Mater.* **2010**, *22*, 1392–1401.
27. Lu, W.; Qu, L.; Henry, K.; Dai, L. High Performance Electrochemical Capacitors from Aligned Carbon Nanotube Electrodes and Ionic Liquid Electrolytes. *J. Power Sources* **2009**, *189*, 1270–1277.
28. Frackowiak, E.; Metenier, K.; Bertagna, V.; Beguin, F. Supercapacitor Electrodes from Multiwall Carbon Nanotubes. *Appl. Phys. Lett.* **2000**, *77*, 2421–2423.
29. Raymundo-Pinero, E.; Leroux, F.; Beguin, F. A High-Performance Carbon for Supercapacitors Obtained from Carbonization of a Seaweed Biopolymer. *Adv. Mater.* **2006**, *18*, 1877–1882.
30. Zhao, L.; Fan, L.-Z.; Zhou, M.-Q.; Guan, H.; Qiao, S.; Antonietti, M.; Titirici, M.-M. Nitrogen-Containing Hydrothermal Carbons with Superior Performance in Supercapacitors. *Adv. Mater.* **2010**, *22*, 5202–5206.
31. Guo, H.; Gao, Q. Boron and Nitrogen Co-Doped Porous Carbon and Its Enhanced Properties as Supercapacitor. *J. Power Sources* **2009**, *186*, 551–556.
32. Han, W.-Q.; Mickelson, W.; Cumings, J.; Zettl, A. Transformation of $B_xC_yN_z$ Nanotubes to Pure BN Nanotubes. *Appl. Phys. Lett.* **2002**, *81*, 1110–1112.
33. Zhi, C. Y.; Bai, X. D.; Wang, E. G. Raman Characterization of Boron Carbonitride Nanotubes. *Appl. Phys. Lett.* **2002**, *80*, 3590–3592.
34. Lee, Y. T.; Park, J.; Choi, Y. S.; Lyu, H.; Lee, H. J. Temperature-Dependent Growth of Vertically Aligned Carbon Nanotubes in the Range 800−1100 °C. *J. Phys. Chem. B* **2002**, *106*, 7614–7618.
35. Bae, S. Y.; Seo, H. W.; Park, J.; Choi, Y. S.; Park, J. C.; Lee, S. Y. Boron Nitride Nanotubes Synthesized in the Temperature Range 1000−1200 °C. *Chem. Phys. Lett.* **2003**, *374*, 534–541.
36. Wang, R. M.; Zhang, H. Z. Analytical TEM Investigations on Boron Carbonitride Nanotubes Grown *via* Chemical Vapour Deposition. *New J. Phys.* **2004**, *6*), 12.
37. McCann, R.; Roy, S. S.; Papakonstantinou, P.; Ahmad, I.; Maguire, P.; McLaughlin, J. A.; Petaccia, L.; Lizzit, S.; Goldoni, A. NEXAFS Study and Electrical Properties of Nitrogen-Incorporated Tetrahedral Amorphous Carbon Films. *Diamond Relat. Mater.* **2005**, *14*, 1057–1061.
38. Zhi, C.; Bando, Y.; Tan, C.; Golberg, D. Effective Precursor for High Yield Synthesis of Pure BN Nanotubes. *Solid State Commun.* **2005**, *135*, 67–70.
39. Won, S.-J.; Suh, S.; Huh, M. S.; Kim, H. J. High-Quality Low-Temperature Silicon Oxide by Plasma−Enhanced Atomic Layer Deposition Using a Metal−Organic Silicon Precursor and Oxygen Radical. *IEEE Electron Devices Lett.* **2010**, *31*, 857–859.